Temperature-dependent evolution of Ti 3*d* spectral features at surface of $Ba_xTi_8O_{16+\delta}$

S. Dash,[1] H. Enomoto,[1] T. Kajita,[2] K. Ono,[3] K. Horiba,[3] M. Kobayashi,[3] H. Kumigashira,[3,4] V. Kandyba,[5] A. Giampietri,[5] A. Barinov,[5] F. Stramaglia,[6] N. L. Saini,[6] T. Katsufuji,[2] and T. Mizokawa[1]

[1]*Department of Applied Physics, Waseda University, Shinjuku, Tokyo 169-8555, Japan*

[2]*Department of Physics, Waseda University, Shinjuku, Tokyo 169-8555, Japan*

[3]*Institute of Materials Structure Science, High Energy Accelerator Research Organization (KEK), Tsukuba, Ibaraki 305-0801, Japan*

[4]*Institute of Multidisciplinary Research for Advanced Materials (IMRAM), Tohoku University, Sendai 980-8577, Japan*

[5]*Sincrotrone Trieste S.C.p.A., Area Science Park, 34012 Basovizza, Trieste, Italy*

[6]*Department of Physics, University of Roma "La Sapienza" Piazalle Aldo Moro 2, 00185 Roma, Italy*

(Received 12 April 2019; revised manuscript received 17 June 2019; published 24 September 2019)

We have studied temperature-driven effects on photoemission spectra of hollandite-type $Ba_xTi_8O_{16+\delta}$ across its metal-insulator transition (MIT) at 220 K by using surface-sensitive photon energies from 27 to 70 eV. The surface Ti 3*d* spectral weight was suppressed and shifted towards higher binding energy from the bulk if the surface was obtained by cleavage above the MIT temperature. The Ti 3*d* spectral weight was recovered once the sample was cooled across the MIT, indicating a transfer of Ti 3*d* electrons from the bulk to the surface across the MIT. The recovered Ti 3*d* spectral shape is consistent with the bulk-sensitive result and indicates strong localization character of the Ti 3*d* electron even in the metallic phase. Resonant photoemission spectroscopy with absorption from the Ti 3*p* core level exhibits resonances of the O 2*p*-Ti 3*d* and O 2*p*-Ti 4*s*, *p* hybridized states. The result suggests that the O 2*p*-Ti 4*s*, *p* hybridization plays a role in the interplay between the bulk and the surface in $Ba_xTi_8O_{16+\delta}$.

DOI: 10.1103/PhysRevB.100.125153

I. INTRODUCTION

Transition-metal oxides exhibit a variety of metal-insulator transitions (MITs) with spin-charge-orbital ordering and fluctuation and have been targets of numerous experimental and theoretical studies [1,2]. With an integer number of 3*d* electrons per site, the on-site electron-electron interaction and ligand-to-metal charge-transfer energy are involved in the description of Mott transitions with spin-charge-orbital degrees of freedom. With a noninteger number of 3*d* electrons per site, mixed-valence states with intersite electron-electron and electron-lattice interactions may undergo spin-density wave or charge-density wave formation across the MIT [1,2]. The electronic states with spin-charge-orbital order or fluctuation are sensitive to external perturbations and are expected to vary between the surface and the bulk [3–6]. In this context, it would be interesting to study surface states of transition-metal oxides with spin-charge-orbital instabilities.

Early transition-metal oxides with mixed valence such as $BaV_{10}O_{15}$, $Ba_{1-x}Sr_xV_{13}O_{18}$, and $Ba_xTi_8O_{16-\delta}$ have been attracting renewed interest due to their interesting interplay between charge-orbital fluctuations and suppression of thermal conductivity [7–10]. Hard x-ray photoemission spectroscopy (HAXPES) studies on the mixed-valence V oxides show that their bulk electronic states in the metallic phase are characterized by pseudogap features near the Fermi level due to electron-electron and electron-lattice interactions [11,12]. The spectral features near the Fermi level tend to be suppressed further in the surface-sensitive photoemission measurement, indicating that the electron-electron and electron-lattice interactions are enhanced at their surfaces [13]. On the other hand, a HAXPES study on $Ba_xTi_8O_{16+\delta}$ has shown polaronic spectral features near the Fermi level for the bulk electronic state even in the metallic phase [14,15]. This observation is related to the studies of polaronic spectral features in various quasi-one-dimensional (q-1D) systems. For example, using surface-sensitive photoemission measurements, the polaronic spectral features were reported in β-$Na_{0.33}V_2O_5$ [16,17] and $(TaSe_4)_2I$ [18–20]. In hollandite $K_2Cr_8O_{16}$ [21–23], the spectral weight at the Fermi level is further suppressed due to its large number of *d* electrons leading to increased Hund's coupling [24]. In $PrBa_2Cu_4O_8$ [25,26], the spectral weight at the Fermi edge is suppressed, probably due to the electron-electron and electron-lattice interaction enhanced in the q-1D Cu-O chain [27]. In $Sr_{14-x}Ca_xCu_{24}O_{41}$ with Cu-O ladders [28–30], complete suppression of the quasiparticle peak was reported [31].

Among the various q-1D transition-metal oxides, hollandite-type $Ba_xTi_8O_{16+\delta}$ undergoes a transition from tetragonal to monoclinic at 220 K with fivefold structural modulation along the Ti-O chain without any signature of dimerization [9]. Below 220 K, the resistivity gradually increases with cooling from 10^{-2} Ω cm and reaches 10^4 Ω cm around 50 K [9]. The tetragonal $Ba_xTi_8O_{16+\delta}$ is reported with $x = 1.13$ and $\delta = 0.14$, and the nominal number of *d* electrons per Ti is ≈0.25. The effect of electronic correlation and electron-lattice interaction would be different between the bulk and the surface in such a complicated Ti oxide with charge-orbital instability. Here, we report a surface sensitive photoemission study on $Ba_xTi_8O_{16+\delta}$ with q-1D transport properties. In this paper, we discuss suppression of the Ti 3*d* spectral weight near the Fermi level which

is different between the bulk and the surface. We also report temperature-driven effects on the valence band of $Ba_xTi_8O_{16+\delta}$ surface across the MIT.

In addition, we discuss resonant photoemission spectroscopy (RPES) on the title system across the Ti $3p \rightarrow 3d$ absorption edge. In typical resonant photoemission spectroscopy, photoemission spectra are taken with photon energies below and above an absorption edge energy of a particular core level. While tracking electronic excitations across the absorption edge, a set of different channels are expected such as normal photoemission, RPES, resonant Auger emission, and normal Auger emission (two-hole valence-band satellite) [32]. In RPES across the particular absorption edge, the spectral weight at the valence band is enhanced due to interference of the direct channel and the autoionization channel [33]. The direct channel in the Ti $3p \rightarrow 3d$ RPES is written as $3p^63d^n + h\nu \rightarrow 3p^63d^{n-1} + e^-$. The autoionization channel can be written as $3p^63d^n + h\nu \rightarrow 3p^53d^{n+1} \rightarrow 3p^63d^{n-1} + e^-$, where $3p^53d^{n+1}$ is the intermediate state of the autoionization channel. The RPES intensity as a function of photon energy is given by the Fano profile [33]. It is reported that the onset of resonance across Ti $3p \rightarrow 3d$ is seen at higher energy than the energy-level separation (36.5 eV) between Ti $3p$ and Ti $3d$ in Ti_2O_3 [34]. In the present study, we observe resonance due to Ti $3p \rightarrow$ O $2p$-Ti $3d$ and O $2p$-Ti $4s, p$ hybridized states while tuning photon energy across the Ti $3p \rightarrow 3d$ absorption edge [35–38]. The resonance behavior shows that O $2p$-Ti $4s, p$ character contributes to the increase in the spectral weight.

II. EXPERIMENT

Single crystals of $Ba_xTi_8O_{16+\delta}$ were grown by using the floating zone method, as reported in the literature [9]. Resonant photoemission spectroscopy measurements across Ti $3p \rightarrow 3d$ absorption edge with excitation energy ranging from 35 to 70 eV were performed at BL-28A of the Photon Factory. The single crystals were cleaved under ultrahigh vacuum of 10^{-8} Pa at 240 K to avoid surface contamination. The valence-band spectra were collected by using an excitation energy of 70 eV for different temperatures across the MIT. Emitted photoelectrons were collected by using an OMICRON-SCIENTA R4000 analyzer. The pass energy was set to 5 eV and the total energy resolution was about 20–40 meV. The energy calibration for each spectrum was done by using the Fermi edge of Au. Space-resolved photoemission spectroscopy measurements were performed at the spectromicroscopy beamline 3.2 of the Elettra synchrotron facility in Italy. The base pressure of the spectrometer was in the 10^{-8} Pa range. The crystals were cleaved at 100 K or at 265 K under ultrahigh vacuum and space-resolved photoemission spectra were taken at several temperatures. Photons at 27 eV were focused by using a Schwarzschild objective. The total energy resolution was set to about 70 meV.

III. RESULTS AND DISCUSSION

Figure 1 shows the valence-band photoemission spectra of $Ba_xTi_8O_{16+\delta}$ using a photon energy of 70 eV at different temperatures across the MIT. The sample was cleaved at

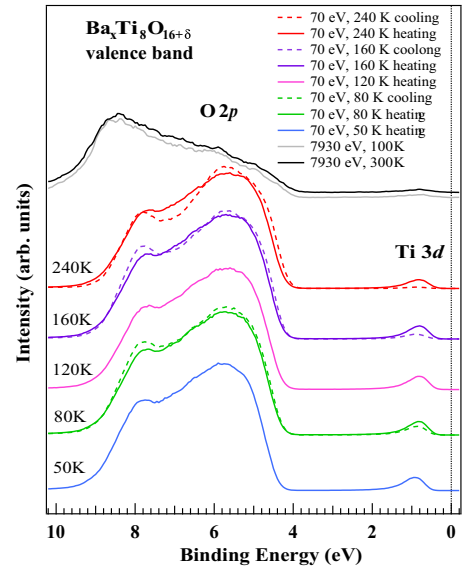

FIG. 1. Valence-band spectra of $BaTi_8O_{16+\delta}$ collected with excitation energy of 70 eV. The valence-band spectra by HAXPES ($h\nu = 7930$ eV) are taken from Refs. [14,15].

240 K under ultrahigh vacuum and the spectra were measured at 240, 160, 80, and 30 K during the cooling process. Since the spectrum at 30 K was considerably affected by the charging effect, the valence-band spectra at 240, 160, and 80 K are plotted for the cooling process in Fig. 1. After that, the spectra were taken at 50, 80, 120, 160, and 240 K in the heating process. In the valence-band region, the O $2p$ bands range from 4 to 9 eV, and the Ti $3d$ band is located at ∼1 eV below the Fermi level. The peaks around 8 and 5 eV are related to O $2p$ orbitals hybridized with Ti $3d$ and Ti $4s, p$ orbitals, respectively [35]. The peak observed at the higher binding energy (≈9 eV) in the bulk-sensitive HAXPES [14,15] is suppressed in the surface-sensitive excitation energy (70 eV). This shows that the 9 eV peak is derived from the Ti $4s$-O $2p$ hybridization since the photoionization cross section of Ti $4s$ is one order of magnitude larger than those of Ti $3d$ and O $2p$ for HAXPES [39]. The spectral weight of Ti $3d$ is strongly suppressed after cleavage at 240 K, as shown by the red dotted curve in Fig. 1. Interestingly, the spectral weight of Ti $3d$ gradually increases with cooling. Once the Ti $3d$ spectral weight is recovered at the lowest temperature, in the heating process, the Ti $3d$ spectral weight does not depend on temperature up to 160 K. This indicates that the electrons are transferred from the bulk to the surface and that the Ti $3d$ electrons are recovered at the surface if the bulk becomes the insulating phase with fivefold superstructure. In going from 160 to 240 K, the Ti $3d$ spectral weight is slightly reduced but never goes back to that after the cleavage. In addition, the peak around 4.5 eV assigned to the nonbonding O $2p$ shows a decrease in its intensity accompanied with increase in the spectral weight at the Ti $3d$ after the temperature cycle, especially at 240 and 160 K (Fig. 1). This indicates that there is a spectral weight transfer from one of the hybridized states to the Ti $3d$ due to possible orbital reconstruction after the cycle.

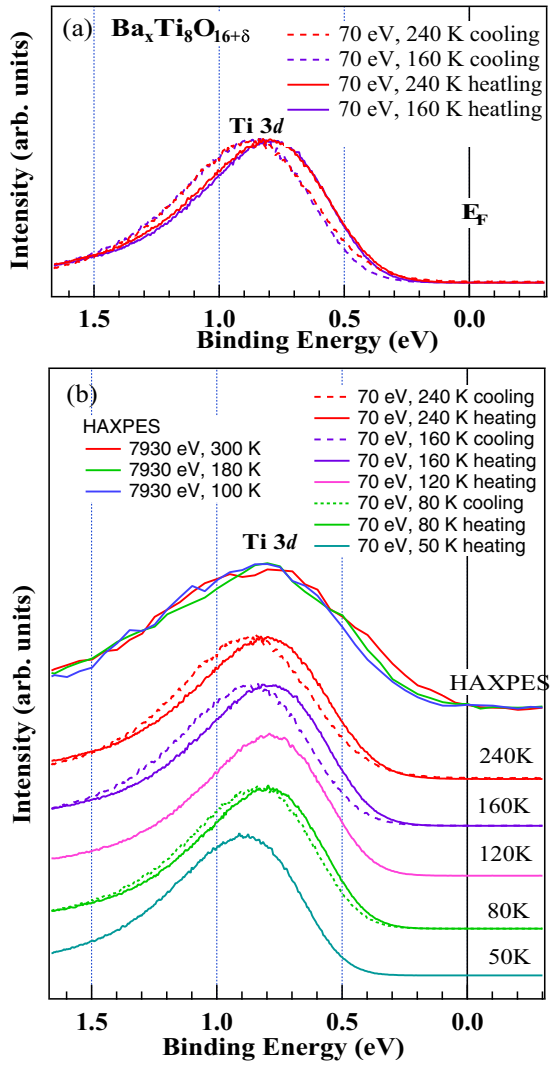

FIG. 2. Ti 3*d* spectra near the Fermi level of $Ba_xTi_8O_{16+\delta}$ collected with excitation energy of 70 eV (a) at 240 and 160 K and (b) across the MIT. The Ti 3*d* spectra by HAXPES ($h\nu = 7930$ eV) are taken from Refs. [14,15].

Figure 2 shows the Ti 3*d* photoemission spectra near the Fermi level of $Ba_xTi_8O_{16+\delta}$ collected at a photon energy of 70 eV. The Ti 3*d* spectra are normalized by peak height to show their energy shift and spectral shape change. In Fig. 2(a), even in the metallic phase at 240 K, the Ti 3*d* spectral weight gradually decreases towards the Fermi level, indicating the strong localization character of Ti 3*d* electrons at the surface. In going from 240 to 160 K across the MIT, the foot of the Ti 3*d* peak shifts away from the Fermi level, which is partly consistent with the MIT in the bulk. However, in the heating process, the Ti 3*d* peak does not change appreciably in going from 160 to 240 K. After the cooling and heating cycle, the Ti 3*d* peak at each temperature is shifted towards the Fermi level, as shown in Figs. 2(a) and 2(b), indicating irreversible change of the surface electronic states. At 50 K where the resistivity is $\sim 10^4$ Ω cm [9], the sample was moderately charged up, and the Ti 3*d* peak shifts away from the Fermi level due to the charging. At 80 K with the resistivity $\sim 10^2$ Ω cm, there was no appreciable charging effect, and the Ti 3*d* peak position after the cooling process is consistent with the HAXPES result at 100 K. Also at 240 K, the Ti 3*d* peak position after the cooling and heating process is more consistent with the HAXPES result than that before the cooling and heating. Therefore, one can safely conclude that the photoemission spectra after the cooling process reflect the intrinsic electronic structure of $Ba_xTi_8O_{16+\delta}$ surface. Here, it should be noted that the Ti 3*d* peak is broader in the HAXPES result due to the poor energy resolution of 270 meV.

Here, let us discuss the bulk and surface electronic states after the cooling process. The surface hosts different electronic properties than the bulk due to a number of possibilities such as surface termination, oxygen defect, structural distortion, and reconstruction. As shown in Fig. 2(b), the bulk sensitive HAXPES spectra at 300 K exhibit the Ti 3*d* spectral weight with its gradual decrease towards the Fermi level. This spectral shape is somewhat consistent with the bad metallic behavior above the MIT temperature. On the other hand, in the surface-sensitive spectra taken at 70 eV, the Ti 3*d* spectral weight is completely suppressed down to 0.3 eV below the Fermi level, indicating that the surface layer is highly insulating although the Ti 3*d* orbitals are partially occupied by electrons. One possibility is that the electron-lattice interaction is enhanced at the surface and the Ti 3*d* electrons are trapped by local lattice distortions such as Ti-Ti dimerization or Jahn-Teller distortion of TiO_6 octahedron at the surface. As for the surface effect just after the cleavage at high temperature, some local distortions may prevent electron transfer from the bulk to the surface, resulting in the suppression of the Ti 3*d* peak. With cooling across the MIT, the phase transition in the bulk would induce structural changes at the surface, and some Ti 3*d* electrons are transferred from the bulk to the surface layer which can be stabilized by Ti-Ti dimerization or Jahn-Teller distortion of TiO_6 octahedron at the surface. Once this stable surface state is formed, it may survive after the temperature cycle.

Figure 3 shows the photoemission spectromicroscopy images of the Ti 3*d* spectral weight and the valence-band spectra of the selected points taken at 27 eV photon energy with 0.6 μm spatial resolution. The Ti 3*d* spectral weight exhibits inhomogeneous distribution as shown in the images. The valence-band spectra taken at 100 and 260 K after the 100 K cleavage are indicated by the broken curves while the solid curves show those taken at 265 and 100 K after the 265 K cleavage. For the 265 K cleavage, the valence-band spectra were taken at four selected points which are indicated by #1, #2, #3, and #4 in the spectromicroscopy image. At 265 K, the Ti 3*d* spectral weight is larger at #1, #2, and #3 than that at #4 which belongs to the dark region in the image. After cooling to 100 K, the specific shape of the crystal edge enabled us to locate the selected points in the spectromicroscopy image at 100 K. When the crystal was cleaved at 265 K and cooled to 100 K, the Ti 3*d* spectral weight increases with cooling at #1, #2, and #3, in qualitative agreement with the data shown in Fig. 1. Since the escape depth is ~3 Å and ~5 Å for the 60–70 and 17–27 eV photoelectrons, respectively [40], the Ti 3*d* peak at 27 eV photon energy is more bulk sensitive and stronger than that at 70 eV photon energy. The temperature dependence of the Ti 3*d* peak position is consistent with the data taken at 70 eV as well as the HAXPES data shown in

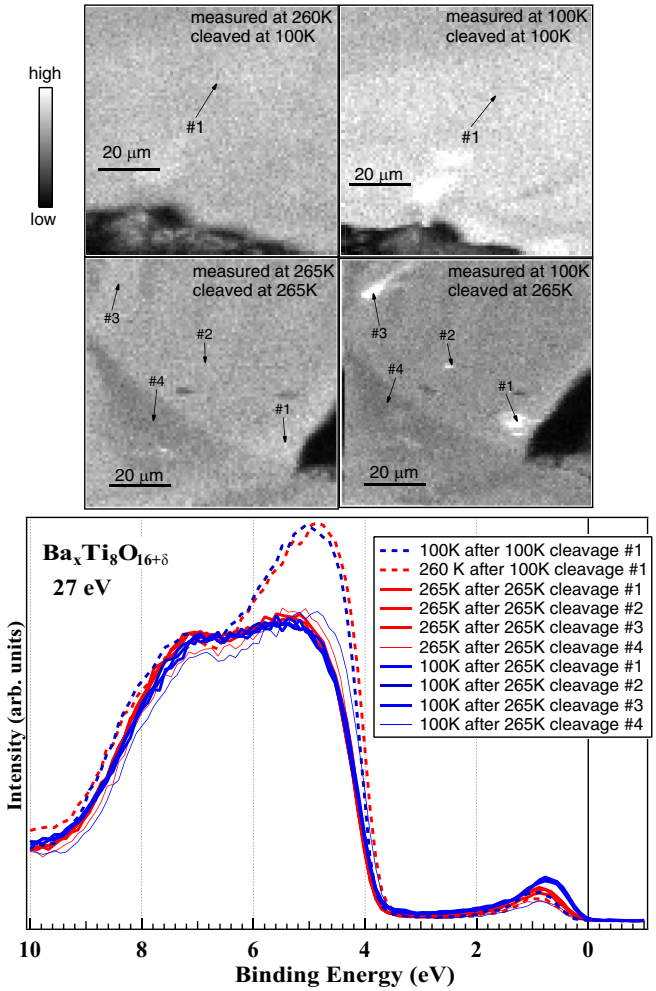

FIG. 3. Photoemission spectromicroscopy images and photoemission spectra taken at 100 and 260 K after the cleavage at 100 K, and those taken at 265 and 100 K after the cleavage at 265 K. The photoemission spectra are measured at the selected points as indicated by #1 for the 100 K cleavage and by #1, #2, #3, and #4 for the 265 K cleavage.

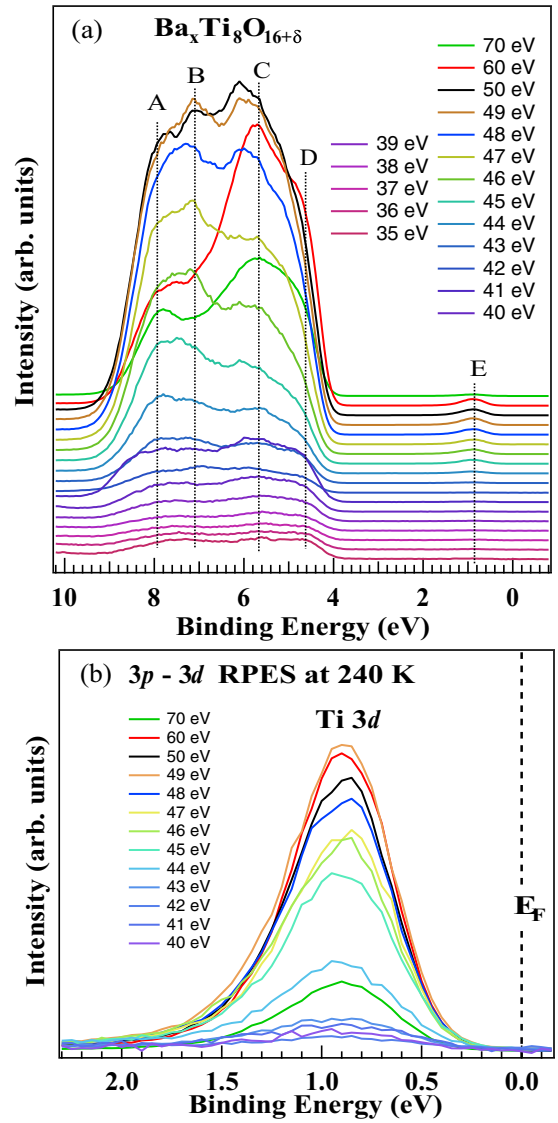

FIG. 4. (a) Resonant photoemission spectra of $Ba_xTi_8O_{16+\delta}$ collected at 240 K. (b) Resonant photoemission spectra of $Ba_xTi_8O_{16+\delta}$ collected at 240 K for Ti 3d area near the Fermi level.

Fig. 2. In the valence-band spectra taken at 27 eV (Fig. 3), the Ti 3d peak is located around 0.9 eV just after the cleavage at 265 K, deviating from the HAXPES result. After the cooling to 100 K, the peak is shifted to ∼0.8 eV at #1, #2, and #3, in agreement with the HAXPES result. Namely, in the surface-sensitive spectra taken at 27 and 70 eV, the Ti 3d peak is at about 0.9 eV after the high-temperature cleave while, after the cooling across the MIT temperature, it is at about 0.8 eV, in agreement with the bulk-sensitive HAXPES. On the other hand, in the spectra at #4 of 265 K cleavage and the spectra for the 100 K cleavage, the Ti 3d spectral weight is relatively small and the Ti 3d peak is located around ∼0.9 eV both at 100 and 265 K (or 260 K), inconsistent with the HAXPES result. Also, the shape of the O 2p band is different when the crystal is cleaved at 100 K.

The resonant photoemission (RPES) across the Ti 3$p \rightarrow$ 3d absorption edge of $Ba_xTi_8O_{16+\delta}$ at 240 K (before the cooling process) is shown in Fig. 4(a). Also, the Ti 3d spectra near the Fermi level are plotted with various photon energies, as shown in Fig. 4(b). The photoemission spectra are normalized by photon flux at each photon energy. Therefore, in addition to the resonance effect, the spectral weight has photon-energy dependence of each subshell. According to the table by Yeh and Lindau [39], the photoionization cross section of Ti 3d is ∼4 Mb at 40 eV and ∼2 Mb at 70 eV, and the photoionization cross section of O 2p is ∼7 Mb at 40 eV and ∼3 Mb at 70 eV. The resonance behavior is shown in Fig. 5(a) where the photoemission intensity is plotted as a function of photon energy of the selected binding energies [points A–E in Fig. 4(a)]. We observe that the intensities of peaks A and B are enhanced with the excitation energy of 50 eV, while the intensities of peaks C and D are enhanced around 60 eV. The two resonance excitation energies of about 50 and 60 eV are derived from the two absorption channels from the Ti 3p core level to the unoccupied O 2p-Ti 3d and O 2p-Ti 4s, p hybridized states, respectively [35,36]. Based on the RPES study across the Ti 3$p \rightarrow$ 3d absorption edge previously

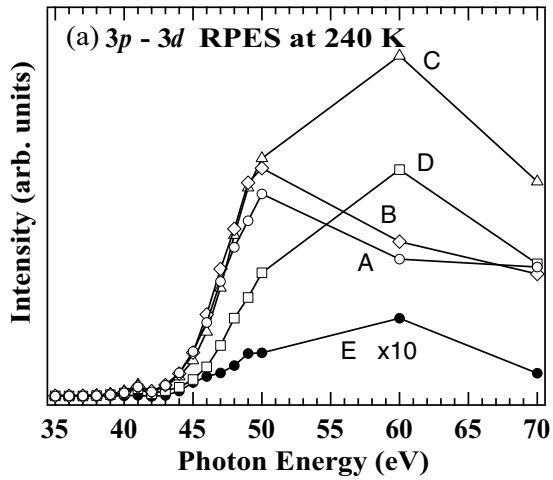

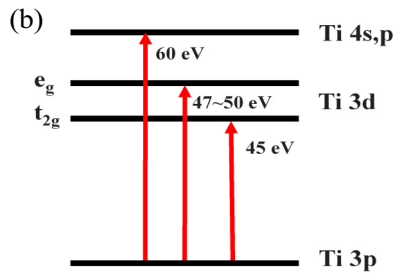

FIG. 5. (a) Photoemission intensity as a function of photon energy for the spectral features labeled A–E. (b) Schematics of absorption from Ti $3p \rightarrow 3d$-O $2p$ and Ti $4s$, p-O $2p$ states.

reported in TiO_2 [35–37], the resonance around 45–50 eV of excitation energy is related to O $2p$-Ti $3d$ whereas the resonance around 60 eV to the O $2p$-Ti $4s$, p hybridized states. This situation is schematically shown in Fig. 5(b). Peaks A and B are related to the Ti $3d$ e_g-O $2p$ and t_{2g}-O $2p$ bonding states. On the other hand, peaks C and D are related to the O $2p$ state, which can hybridize with Ti $4s$, p with less Ti $3d$ contribution [35,37]. Interestingly, peak E or the Ti $3d$ peak exhibits a resonance similar to that of peaks C and D. The weak resonance around 45–50 eV is due to the transition from Ti $3p$ to Ti $3d$ while the enhancement at 60 eV shows that the O $2p$-Ti $4s$, p hybridization character is involved in the Ti $3d$ peak. The Ti $4s$, p orbitals in the neighboring site are mixed in the Ti $3d$ orbitals due to the edge-sharing TiO_6 octahedra. Interestingly, in Ref. [35], the strong Ti $4s$, p resonance was observed in the (110) rutile TiO_2 surface where the edge-sharing Ti-O chain is located at the surface [35]. On the other hand, the Ti $4s$, p resonance is not significant in anatase TiO_2. Since the present hollandite $Ba_xTi_8O_{16+\delta}$ has the edge-sharing Ti-O double chain, the strong Ti $4s$, p resonance commonly observed in rutile and hollandite Ti oxide surfaces is specific to the edge-sharing Ti-O chain. Here, one can speculate that the temperature-driven enhancement of the Ti $3d$ spectral weight at the surface (Fig. 1) would be related to the O $2p$-Ti $4s$, p hybridization, which may help Ti-Ti dimerization or TiO_6 Jahn-Teller distortion in the chain.

IV. CONCLUSION

In the surface-sensitive photoemission study on $Ba_xTi_8O_{16+\delta}$, the Ti $3d$ spectral weight is suppressed just after the cleavage above the MIT and is recovered after the cooling process across the MIT. This observation shows that the Ti $3d$ electron transfer from the bulk to the surface is related to the charge-orbital ordering and fluctuation in the bulk. The Ti $3p \rightarrow 3d$ resonant photoemission shows the strong resonance due to the hybridization of oxygen $2p$ with Ti $3d$ and Ti $4s$, p at the surface. The Ti $3d$ peak shows the resonance due to transitions from Ti $3p$ to unoccupied Ti $3d$ and O $2p$-Ti $4s$, p hybridized states, indicating the contribution of Ti $4s$, p to the spectral weight of the Ti $3d$ peak. Even after the cooling and heating process, the spectral weight near the Fermi level is still reduced below that of the HAXPES result, indicating the stronger localization character of Ti $3d$ at the surface.

ACKNOWLEDGMENTS

The synchrotron radiation experiments were performed with the approvals of KEK-Photon Factory, Tsukuba, Japan (Proposal No. 2015G058) and Elettra, Trieste, Italy (Proposal No. 20180309). This work was supported by CREST-JST (Grant No. JPMJCR15Q2) and KAKENHI from JSPS (Grants No. 19H01853 and No. 19H00659). This work was supported by joint research program of ZAIKEN, Waseda University (Project No. 31010).

[1] M. Imada, A. Fujimori, and Y. Tokura, Rev. Mod. Phys. **70**, 1039 (1998).
[2] D. I. Khomskii, *Transition Metal Compounds* (Cambridge University Press, Cambridge, 2014).
[3] C. N. R. Rao and B. Raveau, *Transition Metal Oxides: Structure, Properties, and Synthesis of Ceramic Oxides*, 2nd ed. (Wiley–VCH, New York and Weinheim, 1998).
[4] P. C. Snijders, M. Gao, H. Guo, G. Cao, W. Siemons, H. Gao, T. Z. Ward, J. Shen, and Z. Gai, Nanoscale **5**, 9659 (2013).
[5] J. Mannhart and D. G. Schlom, Science **327**, 1607 (2010).
[6] S. Dash, T. Kajita, T. Yoshino, N. L. Saini, T. Katsufuji, and T. Mizokawa, J. Electron Spectrosc. Relat. Phenom. **223**, 11 (2018).
[7] T. Kajita, T. Kanzaki, T. Suzuki, J. E. Kim, K. Kato, M. Takata, and T. Katsufuji, Phys. Rev. B **81**, 060405(R) (2010).
[8] M. Ikeda, Y. Nagamine, S. Mori, J. E. Kim, K. Kato, M. Takata, and T. Katsufuji, Phys. Rev. B **82**, 104415 (2010).
[9] R. Murata, T. Sato, T. Okuda, Y. Horibe, H. Tsukasaki, S. Mori, N. Yamaguchi, K. Sugimoto, S. Kawaguchi, M. Takata, and T. Katsufuji, Phys. Rev. B **92**, 220408(R) (2015).
[10] T. Katsufuji, T. Okuda, R. Murata, T. Kanzaki, K. Takayama, and T. Kajita, J. Phys. Soc. Jpn. **85**, 013703 (2016).
[11] T. Yoshino, M. Okawa, T. Kajita, S. Dash, R. Shimoyama, K. Takahashi, Y. Takahashi, R. Takayanagi, T. Saitoh, D. Ootsuki, T. Yoshida, E. Ikenaga, N. L. Saini, T. Katsufuji, and T. Mizokawa, Phys. Rev. B **95**, 075151 (2017).

[12] S. Dash, M. Okawa, T. Kajita, T. Yoshino, R. Shimoyama, K. Takahashi, Y. Takahashi, R. Takayanagi, T. Saitoh, D. Ootsuki, T. Yoshida, E. Ikenaga, N. L. Saini, T. Katsufuji, and T. Mizokawa, Phys. Rev. B **95**, 195116 (2017).
[13] T. Yoshino, K. Wakita, E. Paris, A. Barinov, T. Kajita, T. Katsufuji, V. Kandyba, T. Sugimoto, T. Yokoya, N. L. Saini, and T. Mizokawa, Phys. Rev. B **96**, 115161 (2017).
[14] S. Dash, T. Kajita, M. Okawa, T. Saitoh, E. Ikenaga, N. L. Saini, T. Katsufuji, and T. Mizokawa, Phys. Rev. B **97**, 165116 (2018).
[15] S. Dash, T. Kajita, M. Okawa, T. Saitoh, E. Ikenaga, N. L. Saini, T. Katsufuji, and T. Mizokawa, Phys. Rev. B **99**, 079901(E) (2019).
[16] K. Okazaki, A. Fujimori, T. Yamauchi, and Y. Ueda, Phys. Rev. B **69**, 140506(R) (2004).
[17] T. Yamauchi, Y. Ueda, and N. Mori, Phys. Rev. Lett. **89**, 057002 (2002).
[18] M. Grioni, S. Pons, and E. Frantzeskakis, J. Phys.: Condens. Matter **21**, 023201 (2009).
[19] L. Perfetti, H. Berger, A. Reginelli, L. Degiorgi, H. Höchst, J. Voit, G. Margaritondo, and M. Grioni, Phys. Rev. Lett. **87**, 216404 (2001).
[20] C. Tournier-Colletta, L. Moreschini, G. Autès, S. Moser, A. Crepaldi, H. Berger, A. L. Walter, K. S. Kim, A. Bostwick, P. Monceau, E. Rotenberg, O. V. Yazyev, and M. Grioni, Phys. Rev. Lett. **110**, 236401 (2013).
[21] K. Hasegawa, M. Isobe, T. Yamauchi, H. Ueda, J. I. Yamaura, H. Gotou, T. Yagi, H. Sato, and Y. Ueda, Phys. Rev. Lett. **103**, 146403 (2009).
[22] P. Mahadevan, A. Kumar, D. Choudhury, and D. D. Sarma, Phys. Rev. Lett. **104**, 256401 (2010).
[23] T. Toriyama, A. Nakao, Y. Yamaki, H. Nakao, Y. Murakami, K. Hasegawa, M. Isobe, Y. Ueda, A. V. Ushakov, D. I. Khomskii, S. V. Streltsov, T. Konishi, and Y. Ohta, Phys. Rev. Lett. **107**, 266402 (2011).
[24] P. A. Bhobe, A. Kumar, M. Taguchi, R. Eguchi, M. Matsunami, Y. Takata, A. K. Nandy, P. Mahadevan, D. D. Sarma, A. Neroni, E. Sasioğlu, M. Lezaić, M. Oura, Y. Senba, H. Ohashi, K. Ishizaka, M. Okawa, S. Shin, K. Tamasaku, Y. Kohmura, M. Yabashi, T. Ishikawa, K. Hasegawa, M. Isobe, Y. Ueda, and A. Chainani, Phys. Rev. X **5**, 041004 (2015).
[25] K. Takenaka, K. Nakada, A. Osuka, S. Horii, H. Ikuta, I. Hirabayashi, S. Sugai, and U. Mizutani, Phys. Rev. Lett. **85**, 5428 (2000).
[26] N. E. Hussey, M. N. McBrien, L. Balicas, J. S. Brooks, S. Horii, and H. Ikuta, Phys. Rev. Lett. **89**, 086601 (2002).
[27] T. Mizokawa, C. Kim, Z.-X. Shen, A. Ino, T. Yoshida, A. Fujimori, M. Goto, H. Eisaki, S. Uchida, M. Tagami, K. Yoshida, A. I. Rykov, Y. Siohara, K. Tomimoto, S. Tajima, Yuh Yamada, S. Horii, N. Yamada, Yasuji Yamada, and I. Hirabayashi, Phys. Rev. Lett. **85**, 4779 (2000).
[28] N. Motoyama, T. Osafune, T. Kakeshita, H. Eisaki, and S. Uchida, Phys. Rev. B **55**, R3386(R) (1997).
[29] T. Osafune, N. Motoyama, H. Eisaki, and S. Uchida, Phys. Rev. Lett. **78**, 1980 (1997).
[30] P. Abbamonte, G. Blumberg, A. Rusydi, A. Gozar, P. G. Evans, T. Siegrist, L. Venema, H. Eisaki, E. D. Isaacs, and G. A. Sawatzky, Nature (London) **431**, 1078 (2004).
[31] T. Yoshida, X. J. Zhou, Z. Hussain, Z.-X. Shen, A. Fujimori, H. Eisaki, and S. Uchida, Phys. Rev. B **80**, 052504 (2009).
[32] L. Sangaletti, S. Dash, A. Verdini, L. Floreano, A. Goldoni, G. Drera, S. Pagliara, and A. Morgante, J. Phys.: Condens. Matter **24**, 235502 (2012).
[33] U. Fano, Phys. Rev. **124**, 1866 (1961).
[34] K. E. Smith, Surface and bulk electronic structure and chemisorption properties of Titanium and Vanadium Oxides, Ph.D. thesis, Yale University, 2003.
[35] A. G. Thomas, W. R. Flavell, A. K. Mallick, A. R. Kumarasinghe, D. Tsoutsou, N. Khan, C. Chatwin, S. Rayner, G. C. Smith, R. L. Stockbauer, S. Warren, T. K. Johal, S. Patel, D. Holland, A. Taleb, and F. Wiame, Phys. Rev. B **75**, 035105 (2007).
[36] A. G. Thomas, W. R. Flavell, A. R. Kumarasinghe, A. K. Mallick, D. Tsoutsou, G. C. Smith, R. Stockbauer, S. Patel, M. Grätzel, and R. Hengerer, Phys. Rev. B **67**, 035110 (2003).
[37] Z. Zhang, S-P. Jeng, and V. E. Henrich, Phys. Rev. B **43**, 12004 (1991).
[38] E. Bertel, R. Stockbauer, and T. E. Madey, Phys. Rev. B **27**, 1939(R) (1983).
[39] J. J. Yeh and I. Lindau, At. Data Nucl. Data Tables **32**, 1 (1985).
[40] S. Hüfner, *Photoelectron Spectroscopy: Principles and Applications* (Springer, Berlin and Heidelberg, 2003).